Grain and grain-boundary critical currents in coated conductors with noncorrelating $YBa_2Cu_3O_7$ and substrate grain-boundary networks

A. Palau, T. Puig,[a] and X. Obradors
Institut de Ciència de Materials de Barcelona, CSIC, Campus UAB, 08193 Bellaterra, Spain

R. Feenstra, A. A. Gapud, and E. D. Specht
Oak Ridge National Laboratory, Oak Ridge, Tennessee 37831-6057

D. M. Feldmann
Applied Superconductivity Center, University of Wisconsin—Madison, Madison, Wisconsin 53706

T. G. Holesinger
Los Alamos National Laboratory, Los Alamos, New Mexico 87545

(Received 6 May 2005; accepted 20 December 2005; published online 28 March 2006)

The superconducting grain-boundary (GB) network of coated conductors (CCs) is usually assumed to be a replica of the substrate network. In this letter, we analyze IBAD and RABITS CCs, where such replica either do or do not exist. We have analyzed the effect of GB overgrowth on the critical currents by quantifying the average superconducting grain size and determining the intragrain and grain-boundary critical current densities, J_c^G and J_c^{GB}. We have employed a recently developed inductive methodology enabling the simultaneous determination of these three parameters. We show that the percolative J_c^{GB} may be reduced by 50% if the GB networks do not correlate, while J_c^G and the grain pinning properties appear unaffected. © *2006 American Institute of Physics*.
[DOI: 10.1063/1.2172737]

Coated conductors (CCs) are a new type of superconducting flexible and long length material able to transport high currents through a percolative network of small-angle grain boundaries (GBs).[1–3] It has been shown[4] that the $YBa_2Cu_3O_7$ (YBCO) grains are usually a close replica of the underlying textured substrate and therefore, the grain size ($2a$) and grain-to-grain alignment of the superconducting layers is basically determined by the substrate. CCs grown on Ion-beam-assisted deposition (IBAD) and rolling assisted biaxially textured substrates (RABiTS) hence, are typically characterized by grain sizes of <1 μm and 20–50 μm, respectively.

Recently, it has been reported[5,6] that the *ex situ* BaF_2 YBCO growth process[7,8] may generate YBCO grain structures that deviate from the substrate GB network and thus offer the possibility to study the properties of CCs with and without correlating GB networks. In this process, the YBCO grain size seems to be controlled by laminar growth mediated by a transient liquid phase.[5,9,10]

J_c^G and J_c^{GB} of these CCs have been determined simultaneously by applying the inductive methodology recently reported.[12] These analysis have enabled us to separate the effects of the GB structure and grain size. Zero-field-cooled magnetic hysteresis loops were measured with a Quantum Design 5 T SQUID on samples of 5 mm$\times$5 mm. Subtraction of the substrate magnetic signal was carried out for all samples. The YBCO films were grown by BaF_2 precursor deposited by physical vapor deposition.[7,8] Two films were deposited on IBAD tapes [CeO_2(200 Å)/YSZ ($\sim$1 μm)/hastelloy] and two on the RABiTS architecture CeO_2(150 Å)/YSZ(1500 Å)/Y_2O_3(200 Å)/Ni(1.5 μm)/NiW (3 at .%). For IBAD-1 and RABiTS-1, the YBCO GBs closely replicated the substrate boundaries, whereas IBAD-2 and RABiTS-2 are examples of noncorrelating GB networks. RABiTS-1 and RABiTS-2 were 1 μm and 1.1 μm thick, with average grain sizes of $\sim$20–40 μm and $\sim$50–70 μm, respectively. This difference apparently results from a subtle change in processing, related to a small difference in BaF_2 concentration.[6,13] IBAD-1 was a 1.1 μm thick film containing small YBCO grains, $\sim$0.5–2 μm. By contrast, IBAD-2 was a 2.9 μm thick and showed a bimodal structure where large grains overgrowing the substrate could be identified in the bottom part of the sample ($\sim$60–80 μm) while smaller YBCO grains of about 1 μm were on the top.[5,11] Figures 1(a) and 1(b) show cross-sectional TEM images of IBAD-1 and IBAD-2, respectively, where the different grain structures can be identified. Also, note the presence of a thin intercalated Ba–Cu–O layer between large YBCO grains in IBAD-2.[5] The contrasting grain sizes and GB networks for IBAD-1 and IBAD-2 resulted from an apparently increased role of liquid-mediated growth in thick precursors.[5,6] IBAD-2 was then thinned down to 1.3 μm by ion milling, after which primarily large grains were present in the remaining film. Only results of IBAD-2 after ion milling are reported as an example of a YBCO GB network overgrowing the IBAD GB structure by a large amount. Figures 1(c) and 1(d) show magneto-optical (MO) images of the IBAD-1 and IBAD-2 at 77 K and 60 mT. Figure 1(c) displays a typical MO image of an IBAD CC with grains in the range of the MO resolution, i.e., micron size.[1,14] On the contrary, Fig. 1(d) identifies penetration into a GB network with grains in the range of 50–80 μm.

Inset of Fig. 2, presents the minor $M(H)$of RABiTS-2 as a typical example. As was reported in [12] the maximum of the saturated reversed branch of the magnetization curve of CCs is observed at a positive applied magnetic field. This effect was shown to be a clear confirmation of the magnetic granular structure of a CC attributed to the magnetic field trapped

[a]Electronic mail: teresa.puig@icmab.es

 © 2006 American Institute of Physics
Downloaded 06 Sep 2009 to 160.91.157.167. Redistribution subject to AIP license or copyright; see http://apl.aip.org/apl/copyright.jsp

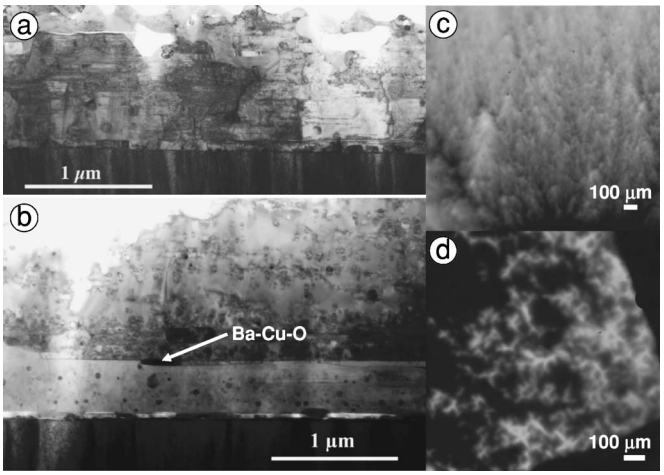

FIG. 1. Cross section TEM images of (a) IBAD-1 and (b) IBAD-2. Vertical striations in the bottom part of both images correspond to different grains in the IBAD-YSZ layer (grain size <1 μm). Different contrast in the YBCO layer in (a) is due to grain-to-grain tilts, indicating a lateral grain size of 0.5–2 μm. Image (b) shows two large YBCO grains stacked along the c axis, separated by an intercalated Ba–Cu–O layer (see Ref. 5). The grains extend beyond the vertical edges of the image. MO images for (c) IBAD-1 and (d) IBAD-2 after zero-field cooling the samples at 77 K and applying 4 60 mT.

inside the grains returning through the GBs, H_{return}. Hence, the local magnetic field at the GBs, $H_{\text{loc}}^{\text{GB}}=H_a\text{-}H_{\text{return}}$. When $H_{\text{loc}}^{\text{GB}}\sim 0$, the magnetization reaches a maximum and $H_{\text{peak}}\sim H_{\text{return}}$. A comparison of the saturated reverse branches of the $M(H)$ curves for the four samples analyzed is shown in Fig. 2. Notice that whereas the four curves exhibit $H_{\text{peak}}^{\text{sat}}$ at $H_a>0$, they all peak at a different H_a: IBAD-1, with the smallest grain size, peaks at 60 Oe, while RABiTS-1, RABiTS-2, and IBAD-2 peak at 320 Oe, 400 Oe, and 440 Oe, respectively. Additionally, the maximum magnetic field that had to be applied in order to saturate the peak position, H_m^{sat} (see inset of Fig. 2), was 450 Oe, 700 Oe, 700 Oe, and 750 Oe for the IBAD-1, RABiTS-1, RABiTS-2, and IBAD-2, respectively. H_m^{sat} is a measure of the magnetic field required to saturate the grains, $H_m^{\text{sat}}\sim H_G^*$, where H_G^* is the full penetration field of the grains. These two experimental magnetic field values, $H_{\text{peak}}^{\text{sat}}$ and H_m^{sat}, can be used to determine J_c^G, and the grain size $(2a)$ by using equations 1 and 2 described in[12] However, by determining the value $g=(H_{\text{peak}}^{\text{sat}}/H_m^{\text{sat}})=(x/2n)/(a/L)$[12] (see Fig. 3 we can directly estimate$(2a)$ (see inset of Fig. 3) , Notice that $(2a)\sim 2$ μm

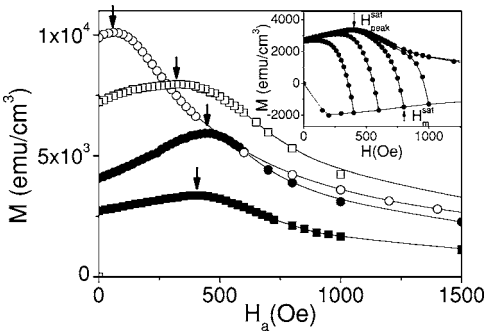

FIG. 2. Saturated reverse branches of M(H) for (○) IBAD-1, (●) IBAD-2, (□) RABiTS-1, and (■) RABiTS-2. $H_{\text{peak}}^{\text{sat}}$, is indicated by arrows. Inset shows minor M(H) of RABiTS-2 at 77 K H_m=400, 600, 800, 1000, 2000, and 5000 Oe. $H_{\text{peak}}^{\text{sat}}$, and H_m^{sat} are indicated.

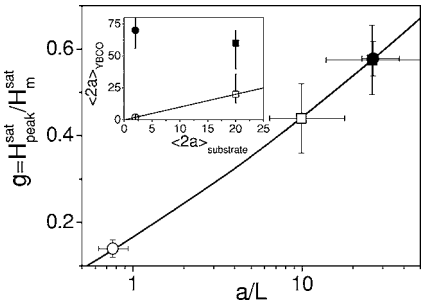

FIG. 3. Theoretical factor $g=H_{\text{peak}}^{\text{sat}}/H_m^{\text{sat}}$ as a function of the cylinder aspect ration a/L (continuous line) (defined in Ref. 12) Superimposed are the experimental g values for (○) IBAD-1, (●) IBAD-2, (□) RABiTS-1, and (■) RABiTS-2. Inset shows the average grain sizes as a function of the average substrate grain size. The solid line indicates substrate grain size equal to YBCO grain size.

and 70 μm for IBAD-1 and IBAD-2, respectively, are in clear agreement with the MO results shown in Fig. 1. We conclude that $2a$ agrees well with that of the substrate textured buffer layer for IBAD-1 and RABiTS-1 samples, whereas there exists significant grain overgrowth for IBAD-2 and RABiTS-2. Hence, we distinguish between two types of YBCO grains: (i) Those originating from a controlled growth process in which grain sizes are determined by the substrate grain size, and (ii) those generated in a growth process with an excess of liquid which produces grains of the order 60–70 μm in both IBAD and RABiTS substrates.

The critical current density at 77 K of these two types of grains $J_c^G=(10/4\pi)H_{\text{peak}}^{\text{sat}}/xL$, being L the film thickness and x a numerically calculated dimensionless factor depending on the ratio a/L,[12] has been determined by calculating the x values i.e., 0.13, 0.83, 1.14, and 1.13 for IBAD-1, RABiTS-1, RABiTS-2, and IBAD-2, respectively. We have obtained similar values of J_c^G for the four samples, J_c^G=3.1 MA/cm^2, 3 MA/cm^2, 2.3 MA/cm^2, and 2.6 MA/cm^2, for IBAD-1, RABiTS-1, IBAD-2, and RABiTS-2, respectively. This indicates that the superconducting properties of both grain types depend only weakly on the grain size, suggesting that the microstructure responsible for vortex pinning is similar in both cases.

In order to determine J_c^{GB}, we use the standard critical state equation for a disk,[12] $J_c^{\text{GB}}=(30\ \text{m}/R_sV_s)$, where m is the value of the magnetic moment at the peak, i.e., $H_{\text{loc}}^{\text{GB}}\sim 0$, and R_s and V_s are the total sample radius and volume, respectively. We have found that J_c^{GB} does depend on the type of GB network, i.e., a YBCO GB network replicating approximately the substrate GB network (IBAD-1 and RABiTS-1) is characterized by $J_c^{\text{GB}}\sim 1.4$ MA/cm^2 while a YBCO GB network overgrowing the substrate (IBAD-2 and RABiTS-2) exhibits about a 50% smaller J_c^{GB}, of 0.67 MA/cm^2 and 0.61 MA/cm^2 for IBAD-2 and RABiTS-2, respectively. This result indicates better performance for current transport in YBCO GB networks propagating from the existing substrate network.

Figure 4 shows the values of J_c^G and J_c^{GB} for the four samples analyzed above and four other samples (two RABiTS closely replicating the substrate GBs and two other with noncorrelating GB networks). We have also included some transport J_c values which agree with the magnetically determined J_c^{GB} values. The additional data confirm a similar J_c^G independent of the GB overgrowth, although there is a decreasing of J_c^G with the sample thickness as already

Downloaded 06 Sep 2009 to 160.91.157.167. Redistribution subject to AIP license or copyright; see http://apl.aip.org/apl/copyright.jsp

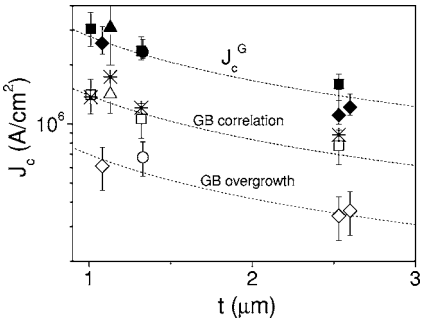

FIG. 4. J_c^G (closed symbols) and J_c^{GB} (open symbols) as a function of the thickness of the YBCO layer, at 77 K, for several RABiTS with replica of the GB network including RABiTS-1 (squares), RABiTS with GB overgrowth; including RABiTS-2 (diamonds), and for IBAD-1 (triangles), and IBAD-2 (circles). Also included are values of the transport for J_c^GRABiTS samples with replica of YBCO GB network (stars).

reported.[7,11] Additionally, for all samples with the YBCO GB network replicating the substrate, we obtain a systematically higher J_c^{GB} than for those with large GB overgrowth. We conclude that the origin of the decrease of the percolative J_c^{GB} of CCs with the large grains is not a decrease in intragrain flux pinning properties, but rather should be attributed to a difference in the GB network. Higher-angle GBs may be induced in these films by a reduced quality of YBCO epitaxy and the presence of intercalated Ba–Cu–O secondary phases.[5] Alternatively, the large grain size indicates a reduced YBCO nucleation density, which could lead to a reduced correlation between grain orientations on a local scale. The strong flux penetration observed by MOI in GBs between large grains for IBAD-2 [Fig. 1(d)] provides evidence of a large difference between J_c^G and J_c^{GB} for this sample, supporting the view that the large grains are connected by relatively large-angle GBs. The systematic differences observed in Fig. 4 suggest that similar mechanisms associated with the formation of the GB network hold for the IBAD and RABiTS templates, underscoring the strong role of transient liquid formation during the growth process.

In summary, we have shown that the percolative, J_c^{GB}, of CCs strongly depends on the details of the growth process in the *ex-situ* BaF_2 method, in particular regarding the role of transient liquid phases. J_c^{GB}, is maximized when the YBCO GB network closely replicates the textured layer underneath. Recent work[6] has shown that in addition to excessive GB overgrowth as discussed here, the GB geometry may change due to the laminar growth mode, leading to meandering of the GB planes. In the case of this meandering, however, the average grain size is maintained through CC architecture, but the average grain size remains small. Excessive liquid phase formation, however, results in large grains and leads to reduced percolative currents J_c^{GB}. By contrast, J_c^G, is controlled by the vortex pinning properties for a given YBCO film thickness, and appears unaffected by variations in the conductor GB network.

Work was supported by CICYT (No. MAT2002-02642), Generalitat de Catalunya (No. 2001-SGR-00336), CeRMAE and EU (No. SOLSULET G5RD-CT2001-00550). A.P. thanks MEC for a doctoral fellowship.

[1] D. Larbalestier, A. Gurevich, D. M. Feldmann, and A. Polyanskii, Nature (London) **414**, 368 (2001).
[2] P. Norton, A. Goyal, J. D. Budai, D. K. Christen, D. M. Kroeger, E. D. Specht, A. He, B. Saffian, M. Paranthaman, C. E. Klabunde, D. F. Lee, B. C. Sales, and F. A. List, Science **274**, 755 (1996).
[3] S. R. Foltyn, P. N. Arendt, P. C. Dowden, R. F. DePaula, J. R. Groves, J. Y. Coulter, Q. Jia, P. Maley, and D. E. Peterson, IEEE Trans. Appl. Supercond. **9**, 1519 (1999).
[4] D. M. Feldmann, J. L. Reeves, A. Polyanskii, G. Kozlowski, R. R. Biggers, R. M. Nekkanti, I. Maartense, M. Tomsic, P. Barnes, C. E. Oberly, T. L. Peterson, S. E. Babcock, and D. C. Larbalestier, Appl. Phys. Lett. **77**, 2906 (2000).
[5] T. G. Holesinger, P. N. Arendt, R. Feenstra, A. A. Gapud, E. D. Specht, D. M. Feldmann, and D. C. Larbalestier, J. Mater. Res. **20**, 1216 (2005).
[6] D. M. Feldmann, D. C. Larbalestier, T. G. Holesinger, R. Feenstra, A. A. Gapud, and E. D. Specht, J. Mater. Res. **20**, 2012 (2005).
[7] R. Feenstra, T. B. Lindemer, J. D. Budai, and D. Galloway, J. Appl. Phys. **69**, 6569 (1991).
[8] R. Feenstra, A. A. Gapud, F. A. List, E. D. Specht, D. K. Christen, T. G. Holesinger, and D. M. Feldmann, IEEE Trans. Appl. Supercond. (to be published).
[9] V. F. Solovyov, H. J. Wiesmann, and M. Suenaga, Physica C **353**, 14 (2001).
[10] P. C. Mcintyre, M. J. Cima, and M. F. Ng, J. Appl. Phys. **68**, 4183 (1990).
[11] D. M. Feldmann, D. C. Larbalestier, R. Feenstra, A. A. Gapud, J. D. Budai, T. G. Holesinger, and P. N. Arendt, Appl. Phys. Lett. **83**, 3951 (2003).
[12] A. Palau, T. Puig, X. Obradors, E. Pardo, C. Navau, A. Sánchez, A. Usoskin, H. C. Freyhardt, L. Fernández, B. Holzapfel, and R. Feenstra, Appl. Phys. Lett. **84**, 230 (2004).
[13] R. Feenstra (unpublished).
[14] C. Jooss, J. Albrecht, H. Kuhn, S. Leonhardt, and H. Kronmuller, Rep. Prog. Phys. **65**, 651 (2002).

Downloaded 06 Sep 2009 to 160.91.157.167. Redistribution subject to AIP license or copyright; see http://apl.aip.org/apl/copyright.jsp